

# Beating stripe solitons arising from helicoidal spin-orbit coupling in Bose-Einstein condensates

Cui-Cui Ding,<sup>1</sup> Qin Zhou,<sup>1,\*</sup> and B. A. Malomed<sup>2,3</sup>

<sup>1</sup>*Research Group of Nonlinear Optical Science and Technology, Research Center of Nonlinear Science, School of Mathematical and Physical Sciences, Wuhan Textile University, Wuhan 430200, China*

<sup>2</sup>*Department of Physical Electronics, School of Electrical Engineering, Faculty of Engineering, and the Center for Light-Matter University, Tel Aviv University, Tel Aviv, Israel*

<sup>3</sup>*Instituto de Alta Investigación, Universidad de Tarapacá, Casilla 7D, Arica, Chile*

(Dated: March 20, 2025)

We demonstrate that the model of a spatially non-uniform two-component Bose-Einstein condensate (BEC) featuring the helicoidal spin-orbit coupling (SOC), gives rise to dark-bright soliton complexes characterized by spatiotemporal periodic oscillations in each component. These solitons are formed by the superposition of dark and bright ones, and exhibit a beating state over time and a striped state across space, earning them the designation of beating stripe solitons. Our analysis demonstrates that helicoidal SOC significantly affects the formation and dynamical properties of these solitons, also serving as the primary driver for spin oscillations. Through the nonlinear superposition of the beating stripe solitons, a range of intricate scenarios of the interaction between multiple solitons emerges, including head-on collisions, bound states, and parallel states.

## I. INTRODUCTION

Vector solitons in multi-component systems have drawn much interest in experimental and theoretical studies due to the great variety of their shapes and properties [1–6]. Owing to their high degree of tunability, multi-component Bose-Einstein condensates (BECs) offer an ideal platform for exploring novel types of vector solitons [7]. In particular, the Manakov system [8], as the vectorial extension of the nonlinear Schrödinger equation, models diverse wave phenomena in fields such as BECs, nonlinear optics, and fluid mechanics, including bright-bright [9], dark-bright [10, 11, 23], and dark-dark solitons [12]. In particular, dark-bright solitons have been studied in detail theoretically [13–19] and created in the experiment [20–23].

The nonlinear superposition of vector solitons typically results in complex coherent or incoherent multi-soliton complexes [24–26], such as non-degenerate solitons [27–29] and beating solitons [22, 30–36]. By utilizing the internal SU(2) symmetry of the system, exact vector-soliton states – specifically, beating ones – can be generated through the superposition of dark-bright solitons [32, 35, 36]. The density distribution of each component of the beating soliton exhibits periodic breathing oscillations, while the total density remains constant [30, 36]. Beating solitons have been experimentally observed in two-component BECs [37]. Numerical simulations have recently shown that the beating solitons exist even in non-integrable systems [38, 39]. Several new types of such solutions have also been discovered in the self-focusing Manakov model [40].

When parameters of a continuous medium are subject to spatially periodic modulation, the translational

invariance is broken, and nonlinear localized excitations usually cannot propagate freely [41, 42]. Several methods have been proposed to support stable moving solitons in periodic media. However, over sufficiently long propagation distances, radiation losses become significant, leading to gradual destruction of the solitons [43–46]. Nevertheless, when a spatially modulated system obeys special symmetries, freely moving nonlinear localized waves, free of radiation losses, persist over indefinitely long distances [47–49], similar to the exact solutions of the Ablowitz-Ladik lattice [50] and some other discrete models [51]. For example, the existence and stability of freely moving solitons in a spatially inhomogeneous BEC with helicoidal spin-orbit coupling (SOC) have been reported [47].

In this paper, we investigate dark-bright soliton complexes featuring spatiotemporal periodic oscillations in a non-uniform two-component BEC under the action of helicoidal SOC. Establishing a gauge equivalence with the Manakov system, we utilize the superposition of bright and dark solitons of the latter system to construct soliton solutions of the former one that exhibit periodic oscillations in both spatial and temporal directions. The density distribution in each individual component of those solitons simultaneously features beating and striped states, whereas the overall density distribution of the system does not exhibit oscillations, therefore, we term these solutions beating stripe solitons (BSSs). We conduct an in-depth analysis of the structure and dynamical behavior of the BSSs, identify existence parameter ranges for different types of solitons, and investigate regularizing effects of the helicoidal SOC on these solitons. Through the analysis of the properties of these solitons, including the particle-density and spin-density distributions, we uncover spin oscillation phenomena. Additionally, we examine interactions between different BSSs, including head-on collisions and their bound and parallel states.

---

\* qinzhou@whu.edu.cn

The subsequent presentation is arranged as follows. The model and its general BSS solutions are presented in Sec. II. In Sec. III, we provide a comprehensive analysis of the generation conditions and dynamical properties of different types of BSSs, along with their three degenerate forms. Specific analysis is presented for the regularizing effects of the helicoidal SOC on the solitons and their relation with spin oscillations. The interactions between BSSs, including the head-on collisions between solitons with different velocities, as well as the bound and parallel states of the solitons with equal velocities, are the subject of Sec. IV. Conclusions are drawn in Sec. V.

## II. MODEL AND FUNDAMENTAL BEATING STRIPE SOLITON (BSS) SOLUTIONS

We consider the one-dimensional spin-1/2 BEC with helicoidal SOC, which is governed, in the mean-field approximation, by the two-component Gross-Pitaevskii (GP) equation, written in the scaled form [47]

$$i\frac{\partial\Psi}{\partial t} = \frac{1}{2}Q^2(x)\Psi - s(\Psi^\dagger\Psi)\Psi. \quad (1)$$

Here the spinor wave function is  $\Psi = (\Psi_1, \Psi_2)^T$ ,  $s = \pm 1$  corresponds to the attractive and repulsive interatomic interactions, respectively, and the helicoidally molded SOC is represented by the generalized momentum operator,

$$Q(x) = -i\partial/\partial x + \alpha\boldsymbol{\sigma} \cdot \mathbf{n}(x) \quad (2)$$

[52–54], with the experimentally tunable SOC strength  $\alpha$ , vector  $\boldsymbol{\sigma} = (\sigma_1, \sigma_2, \sigma_3)$  of the Pauli matrices, and the spatial modulation defined as

$$\mathbf{n}(x) = (\cos(2\kappa x), \sin(2\kappa x), 0), \quad (3)$$

where  $\kappa > 0$  and  $\kappa < 0$  signify the right- and left-handed helicity, respectively [55–57]. Equation (1) with  $\kappa = 0$  correspond to the uniform Rashba-Dresselhaus SOC [58], and to the canonical Manakov system [8] in the case of  $\alpha = 0$ .

Equation (1) for wave function  $\Psi(x, t)$  can be transformed into the standard Manakov system for another spinor wave function,  $\mathbf{u}(x, t)$ . by substitution

$$\Psi = \mathbf{T}\mathbf{u}, \quad (4)$$

with matrix  $\mathbf{T}$  defined by Eq. (A2) in Appendix A, with the determinant  $|\mathbf{T}| = -1$ . We emphasize that, unlike the use of  $SU(2)$  transformations to construct beating solitons, used in previous works [22, 30–36], the transformation matrix here is a function of  $x$ , rather than a constant. This non-uniform transformation, which is determined by the helicoidal SOC, is also the cause of the formation of beating solitons with a striped structure. Therefore, starting from the plane wave as the zero-order seed solution, we can use the transformation, along with

the Darboux transform for the Manakov's system [60], to construct fundamental (first-order) BSS solutions of Eq. (1) in the following compact form:

$$\begin{aligned} \Psi_1 &= e^{-i\kappa x}(\nu_+ u_1 + \nu_- u_2), \\ \Psi_2 &= e^{i\kappa x}(\nu_- u_1 - \nu_+ u_2), \end{aligned} \quad (5)$$

where

$$\begin{aligned} \nu_+ &= \text{sgn}(\alpha)\sqrt{(k_m - \kappa)/(2k_m)} \\ \nu_- &= \sqrt{(k_m + \kappa)/(2k_m)}. \end{aligned} \quad (6)$$

and the dark and bright components are

$$u_j = \rho_j u_{j0} u_j^{db}, \quad (j = 1, 2) \quad (7)$$

with  $u_{j0}$  being the plane waves

$$\begin{aligned} u_{10} &= a \exp i[(k_1 - k_m)x + (sa^2 - \frac{1}{2}k_1^2)t], \\ u_{20} &= \exp i[(k_2 + k_m)x + (sa^2 - \frac{1}{2}k_2^2)t]. \end{aligned} \quad (8)$$

These solutions depend on the amplitude ( $a$ ), wavenumbers ( $k_{1,2}$ ), the effective momentum,  $k_m = \sqrt{\alpha^2 + \kappa^2}$ , and

$$\begin{aligned} \rho_1 &= \sqrt{\frac{(k_1 - \mu_1^*)(k_1 - \mu_2^*)}{(k_1 - \mu_1)(k_1 - \mu_2)}}, \\ \rho_2 &= \frac{l_3}{\sqrt{l_1 l_2}} \sqrt{-4\mu_{1I}\mu_{2I}}. \end{aligned} \quad (9)$$

Additionally

$$\begin{aligned} u_1^{db} &= \frac{\cosh(\Theta_1 + i\epsilon) + \delta \cos(\Theta_2 + i\epsilon) + \gamma_2 \exp(C_1)}{\cosh(\Theta_1) + \delta \cos(\Theta_2) + \gamma_1 \exp(C_1)}, \\ u_2^{db} &= \frac{\cosh(\Theta_3)}{\cosh(\Theta_1) + \delta \cos(\Theta_2) + \gamma_1 \exp(C_1)}, \end{aligned} \quad (10)$$

where

$$\begin{aligned} \Theta_1 &= (\mu_{2I} - \mu_{1I})x + (\mu_{1R}\mu_{1I} - \mu_{2R}\mu_{2I})t + \log \sqrt{\frac{|l_2|^2 \mu_{1I}}{|l_1|^2 \mu_{2I}}}, \\ \Theta_2 &= (\mu_{1R} - \mu_{2R})x + \frac{1}{2}(\mu_{1I}^2 - \mu_{1R}^2 - \mu_{2I}^2 + \mu_{2R}^2)t \\ &\quad + \arg \left[ \frac{l_1^*(\mu_1 - \mu_2^*)}{l_2^*(\mu_1 - \mu_1^*)} \right], \\ \Theta_3 &= -\frac{i}{4}(\mu_1^* - \mu_2^*)[2x - (\mu_1^* + \mu_2^*)t] + \log \sqrt{\frac{l_2^*}{l_1^*}}, \\ C_1 &= -(\mu_{1I} + \mu_{2I})x + (\mu_{1I}\mu_{1R} + \mu_{2I}\mu_{2R})t. \end{aligned} \quad (11)$$

Here,  $*$  stands for the complex conjugate, subscripts  $R$  and  $I$  representing the real and imaginary parts of complex parameters. The relation between eigenvalues  $\mu_{1,2}$  and spectral parameter  $\lambda$  is provided by the quadratic equation:

$$\mu^2 + (2\lambda - k_1)\mu - sa^2 - 2k_1\lambda = 0. \quad (12)$$

Other symbols used in Eq. (10) are

$$\begin{aligned}\epsilon &= \arg\left(\frac{k_1 - \mu_1}{k_1 - \mu_2}\right), \quad \varepsilon = \log\left|\frac{k_1 - \mu_2}{k_1 - \mu_1}\right|, \\ \delta &= \frac{\sqrt{|\mu_1 - \mu_1^*||\mu_2 - \mu_2^*|}}{|\mu_1 - \mu_2^*|}, \\ \gamma_1 &= \frac{s|l_3|^2\sqrt{|\mu_1 - \mu_1^*||\mu_2 - \mu_2^*|}}{4|l_1 l_2|(\lambda^* - \lambda)}, \quad \gamma_2 = \gamma_1/\rho_1.\end{aligned}\quad (13)$$

Solutions (5) describe the spatiotemporal periodically oscillating combination of dark-bright solitons, which exhibits periodic beating in the temporal direction due to the superposition of dark and bright solitons. In the spatial direction, striped states are generated due to the helicoidal SOC, hence we refer to them as BSSs. These solitons are determined by several factors, including the initial background height  $a$ , SOC strength  $\alpha$ , helicity pitch  $\kappa$ , spectral parameter  $\lambda$ , coefficients ( $l_1, l_2, l_3$ ) of the vector eigenfunction, and the nonlinearity coefficient  $s$ . Note that the initial height  $a$  can be fixed as  $a = 1$  by means of a scale transformation.

These solitons encompass two species: the fundamental one, when either  $l_1$  or  $l_2$  is zero, and the composite form, with  $l_{1,2} \neq 0$ . A comprehensive analysis of these solutions is presented in the subsequent section. To reproduce the fundamental form of BSSs from solutions (5), one needs, first, to transform the solution into an expression with a common denominator, and subsequently set  $l_1 = 0$  or  $l_2 = 0$ .

### III. DYNAMICAL PROPERTIES OF BEATING STRIPE SOLITONS (BSSS)

#### A. The general structure of BSSs

In this section, we first consider a simple case of solutions (5) with  $l_1$  or  $l_2$  being zero. To simplify the expressions for the solutions, we set

$$l_1 = 1, \quad l_2 = 0, \quad l_3 = \sqrt{\frac{-2\lambda_{1I}}{s\mu_{1I}}}, \quad (14)$$

and reduce solution (5) to

$$\begin{aligned}\Psi_1 &= e^{-i\kappa x}(\nu_+ \Psi_{DS} + \nu_- \Psi_{BS}), \\ \Psi_2 &= e^{i\kappa x}(\nu_- \Psi_{DS} - \nu_+ \Psi_{BS}),\end{aligned}\quad (15)$$

where the dark and bright solitons,  $\Psi_{DS}$  and  $\Psi_{BS}$ , are

$$\begin{aligned}\Psi_{DS} &= ae^{i\theta'_1} \left[ 1 + \frac{i\mu_{1I}}{k_1 - \mu_1} (1 + \tanh \xi) \right], \\ \Psi_{BS} &= il_3 \mu_{1I} e^{i\theta'_2} \operatorname{sech} \xi,\end{aligned}\quad (16)$$

with

$$\begin{aligned}\xi &= \mu_{1I}(x - \mu_{1R}t), \quad \theta'_1 = -k_m x + \theta_1, \\ \theta'_2 &= (k_m - k_2 + \mu_{1R})x + \frac{1}{2}(k_2^2 + \mu_{1I}^2 - \mu_{1R}^2)t + \theta_2.\end{aligned}\quad (17)$$

Both components  $\Psi_1$  and  $\Psi_2$  described by solutions (15) are formed by the superposition of the dark soliton  $\Psi_{DS}$  and the bright one  $\Psi_{BS}$ , which triggers the emergence of beating solitons on a nonvanishing background. Due to the SOC effect, these solitons simultaneously exhibit the striped state, thus producing the stripe solitons with the beating pattern. Hereafter, we refer to them as BSSs.

To better reveal the dynamic properties and generation mechanism of these BSSs, we first focus on their densities, which can be expressed as

$$\begin{aligned}|\Psi_1|^2 &= a^2 \nu_+^2 + B_1 \operatorname{sech}^2 \xi + a\nu_+ \nu_- \mu_{1I} \Psi_p \operatorname{sech} \xi, \\ |\Psi_2|^2 &= a^2 \nu_-^2 + B_2 \operatorname{sech}^2 \xi - a\nu_+ \nu_- \mu_{1I} \Psi_p \operatorname{sech} \xi,\end{aligned}\quad (18)$$

where

$$\begin{aligned}B_{1,2} &= \mu_{1I}^2 \left[ \nu_{\mp}^2 |l_3|^2 - \frac{a\nu_{\pm}^2}{|k_1 - \mu_1|^2} \right], \\ \Psi_{p_1} &= 2|l_3| \left[ \frac{\mu_{1I} \cos(p_1 + \varsigma_2)}{|k_1 - \mu_1|} (1 + \tanh \xi) - \sin(p_1 + \varsigma_1) \right], \\ \varsigma_1 &= \arg(l_3), \quad \varsigma_2 = \arg[l_3(k_1 - \mu_1)],\end{aligned}\quad (19)$$

and

$$p_1 = k_x x + k_t t \quad (20)$$

with

$$\begin{aligned}k_x &= 2k_m - k_1 + \mu_{1R}, \\ k_t &= \frac{1}{2}(k_1^2 + \mu_{1I}^2 - \mu_{1R}^2),\end{aligned}\quad (21)$$

which characterize the stripe structure and beating states of the solitons. Due to the energy exchange between the two components, the solitons undergo periodic oscillations in the  $x$  and/or  $t$  directions, which is represented by the periodic expression  $\Psi_{p_1}$ .

Solving Eq. (12), we obtained the eigenvalues

$$\mu_{1,2} = \frac{k_1}{2} - \lambda_1 \mp \frac{1}{2}\sqrt{4sa^2 + (k_1 + 2\lambda_1)^2}. \quad (22)$$

To simplify the analysis, we set  $\lambda_{1R} = -\frac{k_1}{2}$  and  $k_2 = 0$  by default hereafter. The BSSs produced by solutions (15) move with the group velocity

$$V_g = \mu_{1R}, \quad (23)$$

which has the specific form  $\mu_{1R} = k_1 - \sqrt{sa^2 - \lambda_{1I}^2}$  for  $sa^2 - \lambda_{1I}^2 > 0$ , while  $\mu_{1R} = k_1$  for  $sa^2 - \lambda_{1I}^2 < 0$ . Based on the general definition of the soliton width and in conjunction with the definition of the width for beating solitons presented in Ref. [36], here we define the width of the BSSs as

$$W = 1/|\mu_{1I}|, \quad (24)$$

which can be written explicitly as  $W = 1/|\lambda_{1I}|$  for  $sa^2 - \lambda_{1I}^2 > 0$  and  $W = 1/|\lambda_{1I} + \sqrt{\lambda_{1I}^2 - sa^2}|$  for  $sa^2 - \lambda_{1I}^2 < 0$ . We stress that  $sa^2 - \lambda_{1I}^2$  is always negative when  $s = -1$ .

TABLE I. Pproperties of the BSSs in both the attractive and repulsive regimes.

Regime	Condition	Velocity $V_g$	Width $W$	Beating period in $t$	Stripe period in $x$	Total density
$s = -1$	$\lambda_{1I} < \sqrt{2}a/4$	$k_1$	$1/ \lambda_{1I} + \sqrt{\lambda_{1I}^2 - sa^2} $	$2\pi/ k_{t1} ^*$	$\pi/ k_m $	Dark soliton
	$\lambda_{1I} > \sqrt{2}a/4$					Bright soliton
	$\lambda_{1I} = \sqrt{2}a/4$					Plane wave
$s = 1$	$sa^2 - \lambda_{1I}^2 \geq 0$	$k_1 - \sqrt{sa^2 - \lambda_{1I}^2}$	$1/ \lambda_{1I} $	$2\pi/ k_{t2} ^\dagger$	$2\pi/ 2k_m - \sqrt{sa^2 - \lambda_{1I}^2} $	Bright soliton
	$sa^2 - \lambda_{1I}^2 \leq 0$	$k_1$	$1/ \lambda_{1I} + \sqrt{\lambda_{1I}^2 - sa^2} $	$2\pi/ k_{t1} ^*$	$\pi/ k_m $	

$$* k_{t1} = -\frac{sa^2}{2} + \lambda_{1I}(\lambda_{1I} + \sqrt{\lambda_{1I}^2 - sa^2}).$$

$$^\dagger k_{t2} = -\frac{sa^2}{2} + \lambda_{1I}^2 + k_1\sqrt{sa^2 - \lambda_{1I}^2}.$$

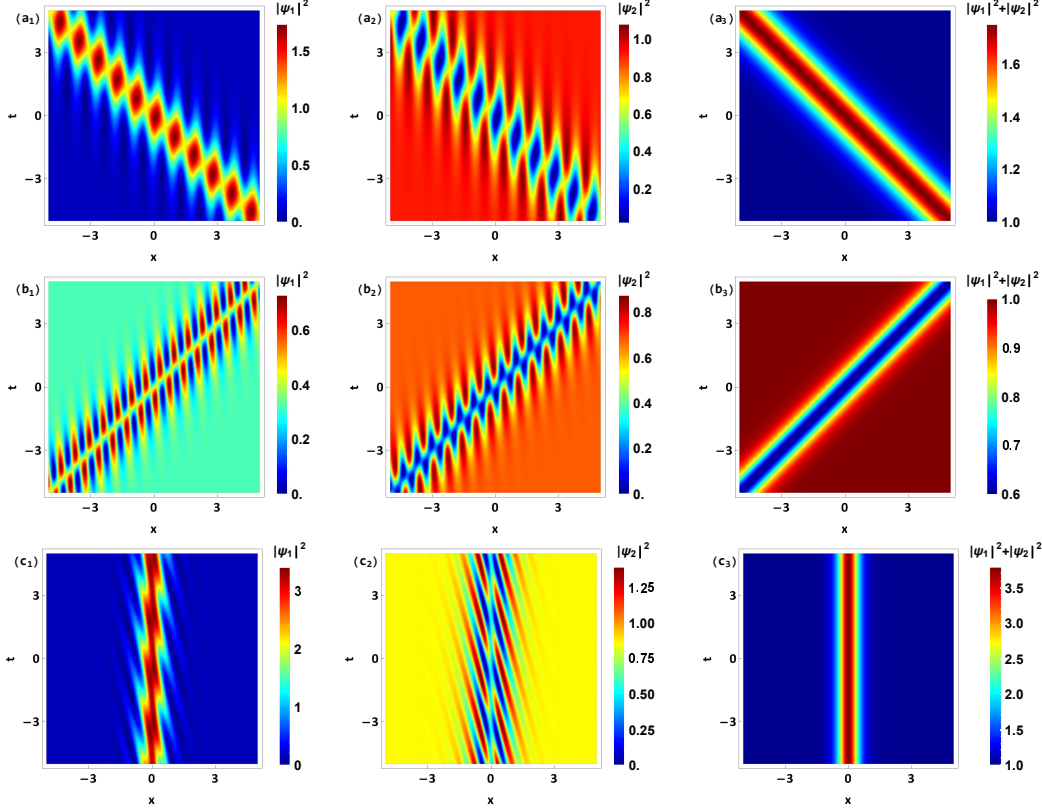


FIG. 1. Beating stripe solitons with different dynamic characteristics in both attraction and repulsion regimes in components  $|\Psi_1|^2$ ,  $|\Psi_2|^2$  and the total density  $|\Psi|^2 = |\Psi_1|^2 + |\Psi_2|^2$ , as produced by solutions (15). (a) A moving soliton in the attraction regime ( $s = 1$ ), with  $k_1 = -\frac{1}{2}$ ,  $\lambda_1 = \frac{1}{4} + \frac{\sqrt{3}}{2}i$ ,  $\alpha = 2$  and  $\kappa = \pi$ . (b) A moving soliton in the repulsion regime ( $s = -1$ ), with  $k_1 = 1$ ,  $\lambda_1 = -\frac{1}{2} + \frac{\sqrt{2}}{6}i$ ,  $\alpha = 4$  and  $\kappa = \frac{\pi}{2}$ . (c) A static soliton in the repulsion regime ( $s = -1$ ) with  $k_1 = 0$ ,  $\lambda_1 = \frac{\sqrt{3}}{2}i$ ,  $\alpha = 3$ , and  $\kappa = \pi$ . The amplitude is  $a = 1$ .

Unlike the periodic oscillations exhibited by the superposition of the dark and bright solitons in a particular component, the total atomic density of the two components does not oscillate. Indeed, using the single-component density in Eq. (18), the total density  $|\Psi|^2 = |\Psi_1|^2 + |\Psi_2|^2$  can be found as

$$|\Psi|^2 = a^2 + \mu_{1I}^2 \left( |l_3|^2 - \frac{a^2}{|k_1 - \mu_1|^2} \right) \text{sech}^2 \xi. \quad (25)$$

The identity relation  $\nu_+^2 + \nu_-^2 \equiv 1$  is used to obtain this

total density. Equation (25) shows that the total density is shaped as a bell-shaped soliton with a nonzero background  $a^2$ , which possesses the same group velocity as the single components. The superposition of the bright and dark solitons results in the two components oscillating in opposite phases. Any protrusion (or depression) in component  $\Psi_1$  mirrors as a depression (or protrusion) in  $\Psi_2$ , maintaining a constant total density and thus giving rise to the BSS.

Dynamical properties of those BSSs in both attractive

and repulsive regimes, including their velocity, width, period, and total density, are given in Table I. From the table, one can obtain the dynamical characteristics of the solitons under different parameter conditions. Specifically, the stripe period of the solitons in the  $x$  direction is directly controlled by the SOC effect, whereas the beating period in the  $t$  direction is only related to spectral parameters. Moreover, in the case of repulsion, the distribution of the total density in the system can exhibit dark/bright soliton forms or even a plane wave, while it always reveals the bright soliton in the case of attraction.

BSSs given by solutions (15) with different dynamic characteristics in both attraction and repulsion regimes are shown in Fig. 1. Analysis of Eq. (25) reveals that, in the attraction regime ( $s = 1$ ), the total amplitude of the two components exceeds the background amplitude  $a$  along the characteristic line  $\xi = 0$ , behaving as a bright soliton, as shown in Fig. 1(a). However, in the repulsion regime ( $s = -1$ ), for  $\lambda_{1I} < \frac{\sqrt{2}}{4}a$ , the total amplitude is less than the background amplitude, exhibiting a dark soliton, as seen in Fig. 1(b), while for  $\lambda_{1I} > \frac{\sqrt{2}}{4}a$  the total amplitude exceeds the background value, looking as a bright soliton, as shown in Fig. 1(c).

Properly adjusting the spectral parameters, we can display BSSs that exhibit diverse propagation characteristics: the backward propagation ( $V_g < 0$ ), forward propagation ( $V_g > 0$ ), and even the stationary behavior ( $V_g = 0$ ), as shown in Figs. 1(a), (b), and (c), respectively. Furthermore, depending on the type and count of extrema within a single periodicity cycle of the BSS, solitons exhibiting distinct configurations emerge, including bright-type solitons (featuring one maximum and two minima), dark-type solitons (featuring one minimum and two maxima), and four-petal solitons, with two maxima and two minima. An extensive variety of combined soliton structures can be produced. As illustrations, we showcase a bright-dark BSS (Fig. 1(a)), a four-petal-four-petal BSS (Fig. 1(b)), and a bright-four-petal BSS (Fig. 1(c)).

### B. Control of beating stripe solitons (BSSs) by the helicoidal SOC

SOC strength  $\alpha$  and helicity pitch  $\kappa$  do not alter the propagation speed of the BSSs, but rather significantly affect their structure. Making use of Eq. (18), one can develop a comprehensive analysis of how the helicoidal SOC modulates the behavior of the BSSs, which feature three types of the degeneration, as illustrated by Fig. 2. Two of the degenerate types manifest themselves as bright-dark soliton pairs, with one exhibiting oscillations in the  $x$  and/or  $t$  directions, while the other remains oscillation-free in those directions, as shown in Figs. 2(a) and (b). The other type is built as a pair of the complementary beating solitons, with the amplitude of the two components equals the background amplitude  $a$ , as shown in Fig. 2(c). The formation of the oscillatory bright-dark

soliton pairs displayed in Fig. 2(a) occurs under the degenerate condition, in which the soliton's characteristic line  $\xi = 0$  is parallel to the oscillation direction  $p_1 = 0$  – specifically, at  $k_t/k_x = -\mu_{1R}$ , which is represented by parameters  $k_m$  (including  $\alpha$  and  $\kappa$ ),  $\lambda_1$  and  $k_1$ . Conversely, the non-oscillatory bright-dark soliton pairs displayed in Fig. 2(b) may solely emerge when both  $k_x$  and  $k_t$  in periodic term (20) simultaneously vanish, in the specific case of  $k_m \equiv \sqrt{\alpha^2 + \kappa^2} = \sqrt{sa^2 - \lambda_{1I}^2}/2$  and  $k_1 = \frac{sa^2 - 2\lambda_{1I}^2}{2\sqrt{sa^2 - \lambda_{1I}^2}}$ . Analysis reveals that this degenerate case occurs solely in the attraction regime ( $s = 1$ ). To produce the two complementary BSSs shown in Fig. 2(c), both  $\lambda_{1I} = \frac{\sqrt{2}}{4}a$  and repulsion regime ( $s = -1$ ) must take place. Such a degenerate case is not possible in the attraction regime. Specific parameter conditions for producing these three kinds of the degenerate BSSs are given in Table II.

TABLE II. Parameter conditions for producing the three kinds of degenerate beating stripe solitons.

Three degenerate cases	Conditions
Bright-dark soliton pair with vibration	$k_t/k_x = -\mu_{1R} \ (s = \pm 1)$
Bright-dark soliton pair without vibration	$k_m = \sqrt{sa^2 - \lambda_{1I}^2}/2,$ $k_1 = \frac{sa^2 - 2\lambda_{1I}^2}{2\sqrt{sa^2 - \lambda_{1I}^2}} \ (s = 1)$
Complementary soliton	$\lambda_{1I} = \frac{\sqrt{2}}{4}a \ (s = -1)$

The SOC effect modulates the spatial oscillation frequency of the beating solitons, resulting in the formation of stripe states, as is evident from Fig. 3. The modulation period in the spatial  $x$  direction is  $2\pi/k_x$ . Typically, the stripes of beating solitons exhibit asymmetry with respect to the  $x$ - and  $t$ -axes. However, under specific conditions, a symmetric configuration can emerge. Our analysis reveals that the beating solitons with symmetric stripes are exclusively observed in attraction regime ( $s = 1$ ) under condition

$$\lambda_{1I} \leq -|a|. \quad (26)$$

Figures 3(a) and (b) showcase a remarkable example of such a bright-dark beating soliton with symmetric stripes. In this system, one component manifests itself as a bright soliton, while the other assumes is a dark soliton. The character of each soliton component is determined by the relative magnitude of SOC intensity  $\alpha$  and rotation frequency  $\kappa$  (actually, by their ratio  $\varpi = \frac{\kappa}{\alpha}$ , as shown in Fig. 3(c). Under a certain symmetry condition, *viz.*,  $s = 1$ ,  $a = 1$  and  $\lambda_{1I} = -1$ , the densities of the two components at  $(x, t) = (0, 0)$  are calculated as

$$\begin{aligned} |\Psi_{10}|^2 &= 1 + \frac{\varpi}{\sqrt{1 + \varpi^2}}, \\ |\Psi_{20}|^2 &= 1 - \frac{\varpi}{\sqrt{1 + \varpi^2}}, \end{aligned} \quad (27)$$

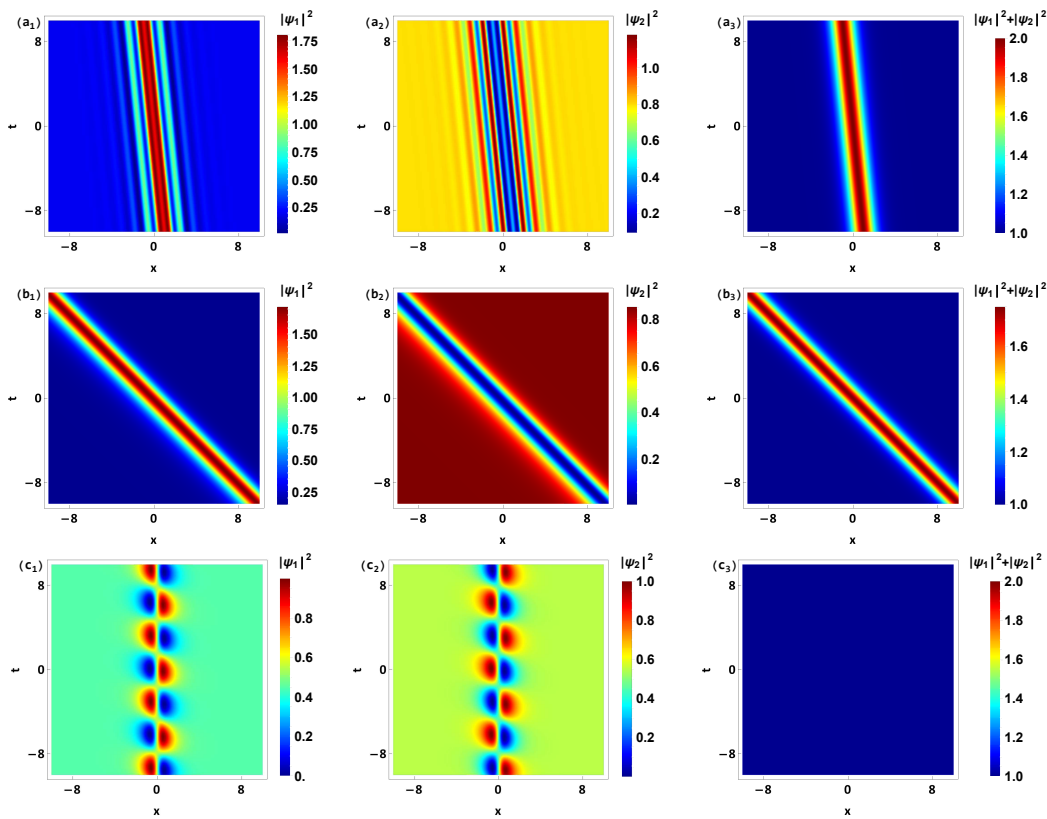


FIG. 2. Three degenerate beating solitons obtained from solutions (15). (a) A bright-dark pair with vibrations in the attraction regime ( $s = 1$ ), with  $k_1 = -0.1$ ,  $\lambda_1 = 0.05 - i$ ,  $\alpha = 2$ , and  $\kappa = \frac{3}{2}$ . (b) A bright-dark pair without vibrations in the attraction regime ( $s = 1$ ), with  $k_1 = -\frac{1}{2}$ ,  $\lambda_1 = \frac{1}{4} + \frac{\sqrt{3}}{2}i$ , and  $\alpha = \kappa = \frac{\sqrt{2}}{8}$ . (c) Complementary beating solitons with a constant total amplitude in the repulsion regime ( $s = -1$ ), with  $k_1 = 0$ ,  $\lambda_1 = \frac{\sqrt{2}}{4}i$ ,  $\alpha = 0.1$ , and  $\kappa = 0.01$ .

with background heights  $|\Psi_{1a}|^2 = [1 + (\varpi + \sqrt{1 + \varpi^2})^2]^{-1}$  and  $|\Psi_{2a}|^2 = 1 - |\Psi_{1a}|^2$ . Their evolution with the change of ratio  $\frac{\kappa}{\alpha}$  is represented in Fig. 3(c). By comparing these values, one can unambiguously classify the soliton as either bright or dark one. Remarkably, the critical threshold for the transition between the bright and dark solitons is identified as  $\varpi = \pm \frac{\sqrt{2}}{4}$  (red points in Fig. 3(c)). When  $\varpi > \frac{\sqrt{2}}{4}$ , we observe a bright-dark BSS. Conversely, when  $\varpi < -\frac{\sqrt{2}}{4}$ , a dark-bright BSS emerges. The intermediate range represents a transition state, where the solitons exhibit a blend of bright and dark characteristics.

To complete the discussion on general BSSs, we finally consider two special cases: (i)  $\kappa = 0$  but  $\alpha \neq 0$  but  $\alpha \neq 0$  (corresponding to the Rashba-Dresselhaus SOC), and (ii)  $\alpha = 0$  (corresponding to the conventional BEC). For the first case, from the density distribution of the two components given by Eq. (18) in conjunction with Eqs. (20) and (21), it can be seen that the fact whether  $\kappa$  is zero or not does not fundamentally affect the structure of the BSSs; however, its sign (corresponding to the right- and left-handed helicity) does determine if the two

components appear as bright or dark structures. In the second scenario, when  $\alpha = 0$  (in which case the value of  $\kappa$  becomes irrelevant), system (1) degenerates into the standard Manakov system. Using the method described in this work, the resulting solutions are typical non-oscillating dark-bright soliton pairs.

### C. Spin oscillations

Eq. (1) is integrable in the absence of the Zeeman splitting [47], and, consequently, it ought to possess an infinite number of conservation laws that fundamentally constrain the system's dynamics, albeit these laws seemingly remain unidentified to date. Here, we delve into the examination of various physical quantities associated with the wave function of the helicoidal SO-coupled BEC system, including the particle density and spin density, also scrutinizing the influence of parameters such as SOC strength  $\alpha$  and helical pitch  $\kappa$  on these quantities. The particle density  $n(x, t)$  and spin density  $\mathbf{f}(x, t)$  of the

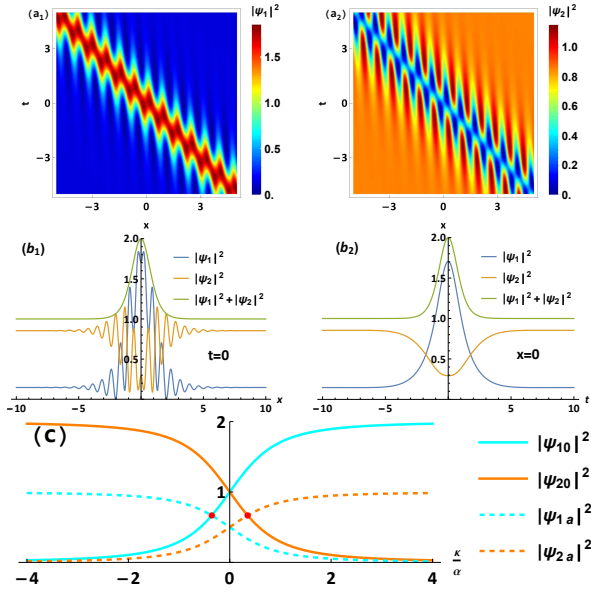


FIG. 3. (a) and (b) The density distribution of beating solitons with symmetric stripes and their symmetric evolution along the directions of  $t = 0$  and  $x = 0$ , with  $\alpha = \kappa = 3$ . (c) The amplitudes of the central stripes  $|\Psi_{j0}|^2$  and background heights  $|\Psi_{ja}|^2$  of the two components vs. ratio  $\frac{\kappa}{\alpha}$ . The red dot corresponds to the transition between the bright and dark solitons. The other parameters are  $s = 1$ ,  $a = 1$ ,  $k_1 = -1$ , and  $\lambda_1 = \frac{1}{2} - i$ .

system are defined as

$$\begin{aligned} n(x, t) &= \Psi^\dagger \cdot \Psi - \Psi[0]^\dagger \cdot \Psi[0], \\ \mathbf{f}(x, t) &= \Psi^\dagger \cdot \boldsymbol{\sigma} \cdot \Psi, \end{aligned} \quad (28)$$

where  $\Psi[0]$  is the initial wave vector given by the seed solutions (A5) and gauge transformation (A2),  $\boldsymbol{\sigma} = (\sigma_1, \sigma_2, \sigma_3)$  are the Pauli matrices and spin density  $\mathbf{f}(x, t) = (f_x, f_y, f_z)$ . In Fig. 4, we present the physical properties of the wave function of BSSs. Due to the fact that the parameters satisfy the symmetry condition (26), it is observed that the soliton stripes are now symmetric, as shown in Fig. 4(a). From Eq. (28), it is also seen that the particle density distribution  $n(x, t)$  takes the form of a soliton, as seen in Fig. 4(b). The spin density distribution  $(f_x, f_y, f_z)$  exhibits some noteworthy features: with the SOC strength  $\alpha \neq 0$  while helical pitch  $\kappa = 0$ , i.e., when SOC is spatially uniform in the system, the spin density distributions in all three directions exhibit oscillations near  $x = 0$  and then tend towards a constant distribution at  $x \rightarrow \pm\infty$ . Among these,  $f_x$  and  $f_z$  are even functions, while  $f_y$  is an odd one, as shown in Fig. 4(c).

Additionally, SOC strength  $\alpha$  and helicity pitch  $\kappa$  have a significant effect on the distribution of spin density, as shown in Fig. 5. We first increase  $\alpha$  while keeping  $\kappa = 0$ . Then, it is observed that the spin density distribution oscillates more intensely near  $x = 0$ , although it eventually

tends towards a constant value. However, for  $\kappa \neq 0$ , i.e., when SOC is non-uniform in the system, spin densities  $f_x$  and  $f_y$  maintain periodic oscillations and do not tend towards constant values, as shown in Fig. 5(b). This is significantly different from the spin-density distributions in the systems with uniform SOC or without SOC. We also find that the increase of the helicity pitch  $\kappa$  leads to increase of the oscillation frequency of the spin density.

#### D. The composite form of the beating stripe soliton (BSS)

When all parameters  $l_j$  ( $j = 1, 2, 3$ ) are different from zero, solutions (5) characterize the general form of a composite BSS, with both components featuring a breather and a BSS. The total density of the components, as a whole, exhibits characteristics akin to both a breather and a soliton.

Figure 6 depicts several varieties of such solitons. Analysis reveals that, at  $sa^2 - \lambda_{1I}^2 > 0$ , the breather propagates periodically parallel to the  $x$ -axis, until it encounters a BSS, resulting in a transformed BSS that alters its direction of propagation, as shown in Fig. 6(a). As depicted and analyzed in Fig. 2(a), when the parameters fulfill the condition  $k_t/k_x = -\mu_{1R}$ , the BSS degenerates into an oscillating bright-dark soliton pair. Subsequently, we can obtain a composite BSS, which is a union of a breather and the oscillating bright-dark soliton pair, as illustrated in Fig. 6(b). Notably, the oscillating bright-dark soliton pair here displays a pronounced oscillation period and, due to the swift decay of the amplitude decay to the background plane, it assumes an  $M$ -shaped form. Despite this, the total density of the two components maintains its shape, consisting of a breather and a soliton. Additionally, it is evident that, upon the collision with the breather, this  $M$ -shaped bright-dark soliton pair evolves into a conventional BSS. Here, the period of the stripe solitons can be controlled by adjusting SOC, thereby changing the number of stripes to form  $M$ -shaped solitons or other forms of stripe solitons. Moreover, in the scenario with  $sa^2 - \lambda_{1I}^2 < 0$ , the breather and the beating soliton keep their parallel alignment, and it is possible to fine-tune the distance between them by adjusting parameter  $l_j$ . A characteristic example showcasing this phenomenon is depicted in Fig. 6(c). Essentially, the ratio  $|l_2|/|l_1|$  plays the role of a modulator, allowing one to adjust the horizontal coordinate of the intersection point between the breather and BSS, whereas  $|l_3|/|l_1|$  serves to alter the vertical position of this point. Accordingly, the positions of the interaction between the soliton and breather can be controlled too. This principle holds true for a diverse array of composite BSSs.

To complete the discussion of BSSs, we conduct numerical simulations to study their stability. By using the split-step Fourier method and the fourth-order Runge-Kutta method, with the analytical solutions (15) as the initial solution, the evolution of BSSs under a 2% noise

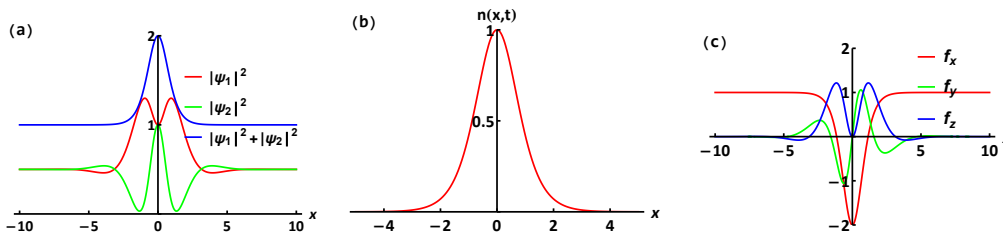


FIG. 4. Physical properties of the wave functions for the beating stripe solitons at instant  $t = 0$ . (a) The local density; (b) The particle density; (c) The spin density. The parameters are  $s = 1$ ,  $a = 1$ ,  $k_1 = 0$ ,  $\lambda_1 = -i$ ,  $\alpha = 0.5$ , and  $\kappa = 0$ .

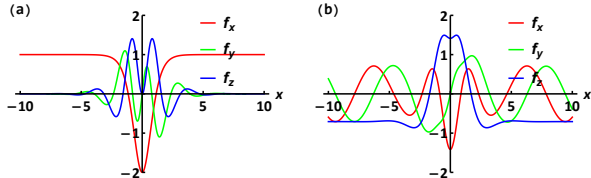


FIG. 5. The role of (a) SOC strength  $\alpha$  and (b) helicity pitch  $\kappa$  in modulating the spin density with  $\alpha = 1$  and  $\kappa = 0$  in (a) and  $\alpha = 0.5$  and  $\kappa = 0.5$  in (b). The other parameters are the same as Fig. 4.

perturbation is obtained. The results are shown in Fig. 7. It can be seen that the basic BSSs in the attractive and repulsive regimes, as well as the non-oscillating bright-dark soliton pairs, can remain basically stable under certain perturbations.

Lastly, it is relevant to compare the present results with previous studies of stripe solitons in the presence of the helicoidal SOC-BEC. The existence and stability of freely moving bright stripe solitons, induced by the linear superposition of bright-bright solitons and the stripe state, were addressed in Ref. [47] (see Eq. (5) of Ref. [47]). In contrast, the present paper primarily examines solitons in the helicoidal SOC-BEC that feature both stripe and beating states, formed by the superposition of dark-bright solitons on the non-zero background.

#### IV. NONLINEAR SUPERPOSITION OF THE BEATING STRIPE SOLITONS (BSSS)

##### A. The nonlinear superposition of the fundamental BSSs

In this subsection, we conduct address the nonlinear superposition of BSSs through the  $N$ -th-order solutions derived in Appendix B, and analyze the interaction between the two solitons. Firstly, we consider the attraction regime with  $s = 1$ . In this particular scenario, the velocities of the two solitons can vary, depending on the choice of spectral parameters  $\lambda$ . Specifically, for  $sa^2 - \lambda_j^2 \geq 0$ , the velocity is  $V_g = k_1 - \sqrt{sa^2 - \lambda_j^2}$ , whereas for  $sa^2 - \lambda_j^2 \leq 0$  it is  $V_g = k_1$ . To study the interaction between different solitons, we manipulate one

soliton to exhibit both beating and striped states simultaneously, while modifying the morphology of the other soliton, including the BSS, the stripe soliton lacking a beating pattern, and the single soliton without any beating or striping. Illustrative examples of head-on collisions involving various types of BSSs are displayed in Fig. 8. It is evident that, although solitons maintain their beating and/or stripe states after interaction, there are subtle changes in their shapes, in addition to the interaction-induced phase shift.

In addition to the head-on collision that occurs when solitons travel at different speeds, bound solitons can be formed when two solitons possess identical velocities. Under such circumstances, the two BSSs assume a bound or parallel state, as shown in Fig. 9. In the attraction regime, we can take  $\lambda_{1,2I} \geq 1$  to obtain two solitons with identical velocities  $V_g = k_1$ ; then, the BSS with a bound or parallel state can emerge. In the case of repulsion, given that the velocity of the solitons remains constant and equivalent to  $k_1$ , the two solitons invariably form the bound or parallel state, as illustrated in Fig. 9. When the distance between the two solitons is relatively short (adjustable via  $l_1$ ), a periodic bound state, characterized by alternating attraction and repulsion can be observed, as shown in Figs. 9 (a) and (b). Conversely, when the solitons are situated farther apart, they maintain a parallel arrangement, as shown in Fig. 9 (c). It is worth pointing out that SOC strength  $\alpha$  and helicity pitch  $\kappa$ , which have no impact on the velocity of soliton, do not affect their bound or parallel states either. Instead, they merely modify the solitons' inherent beating and stripe states. BSSs, which are parallel to each other with a bright total density in the attraction regime, can also be obtained by adjusting the distance between the two solitons when they possess the same velocity.

##### B. The nonlinear superposition of the composite BSS

Next, we delve into a more comprehensive scenario involving the nonlinear superposition of two composite BSSs, thereby investigating their interactions. In this context, all coefficients  $l_{ij}$  are different from zero. Initially, we examine a scenario where the solitons inter-

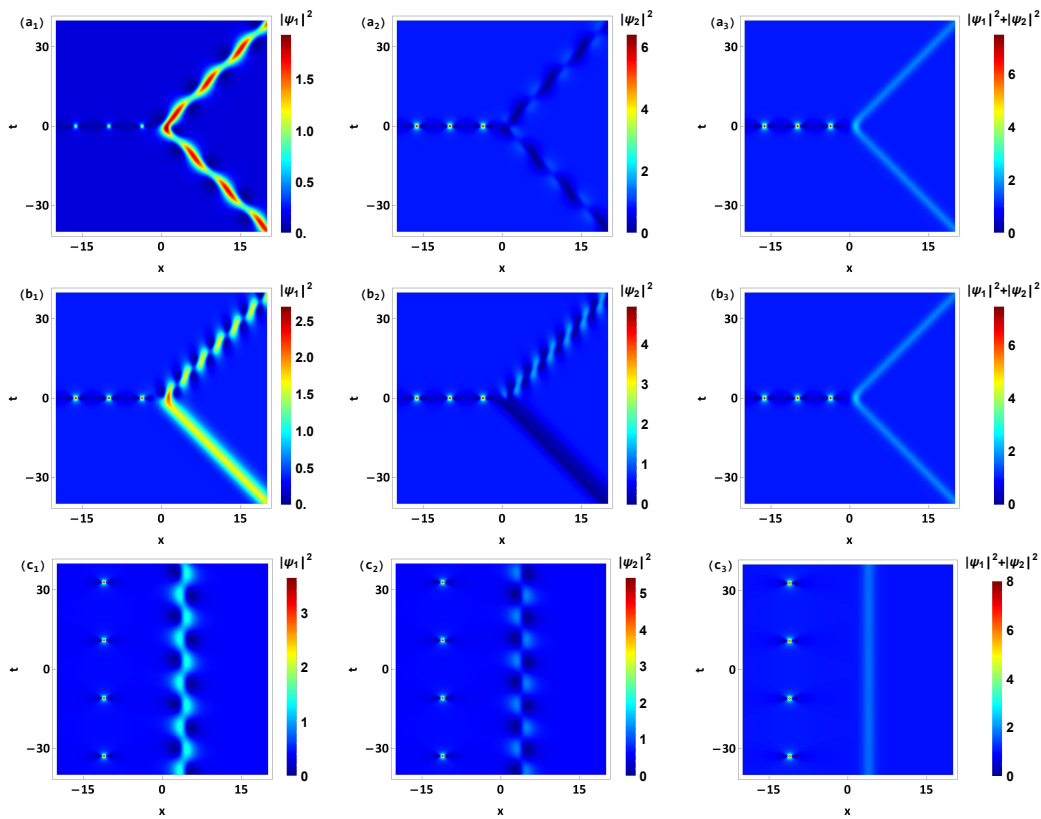


FIG. 6. Density distributions of various composite beating stripe solitons given by solutios (5) with parameters (a)  $\lambda_1 = \frac{\sqrt{3}}{2}i$ ,  $\alpha = \kappa = 0.01$ ,  $l_1 = l_2 = l_3 = 1$ ; (b)  $\lambda_1 = \frac{\sqrt{3}}{2}i$ ,  $\alpha = 0.48$ ,  $k_m = 0.5$ ,  $l_1 = l_2 = l_3 = 1$ ; (c)  $\lambda_1 = 1.01i$ ,  $\alpha = 0.05$ ,  $\kappa = 0.01$ ,  $l_1 = l_3 = 1$ ,  $l_2 = 20$ . The other parameters are  $s = 1$ ,  $a = 1$ ,  $k_1 = 0$ .

sect rather than align in parallel, with the directions of the two solitons configured to be opposite. This setup is illustrated in Fig. 10(a). In the attraction regime, one soliton exclusively exhibits a stripe shape, devoid of a beating state, while the other soliton carries both the beatings and stripe structure. Notably, the interaction between the two Y-shaped solitons, oriented in diverging directions, generates a hexagon at their junction, which is composed of (beating) stripe solitons and breathers. The interaction is quasi-elastic, as both types of solitons and the breather retain their structures intact post-interaction.

Next, we examine the interactions between two parallel composite solitons in the attraction regime, as shown in Figs. 10(b) and (c). When the imaginary part of the spectral parameter  $\lambda$  is  $\geq 1$ , the two composite solitons share the same velocity and maintain their parallel alignment. Additionally, the distance between the soliton and breather can be adjusted by varying the values of  $l_{ij}$ . Notably, in the case of  $\text{Im}(\lambda) = 1$ , one component degrades, featuring solely BSS without a breather, as illustrated in Figs. 10(c). Similar properties are demonstrated by interactions between other types of composite solitons.

## V. CONCLUSIONS

In summary, we have investigated the BSSs (beating stripe solitons) in the two-component BEC under the action of the non-uniform helicoidal spin-orbit coupling (SOC). By establishing the possibility of its transformation to the integrable Manakov system, we have constructed fundamental and  $N$ -th order soliton solutions for the original BEC system, in the case of both attractive and repulsive interactions. These solutions describe spatial and/or temporal periodic breathing oscillations of the density distribution in each component, which simultaneously possess beating and striped phases, while the total density does not exhibit oscillations. Solutions for various moving and static bright/dark/four-petal solitons, along with three degenerate forms, including bright-dark soliton pairs with or without oscillations and complementary beating solitons, were obtained. We have conducted the analysis of the propagation dynamics and established parametric conditions for the existence of such solitons. Further analysis revealed that helicoidal SOC significantly affects the structure of such solitons. Conditions for the generation of symmetric and asymmetric BSSs were reported too. In the study of physical quantities, such as the particle and spin densities,

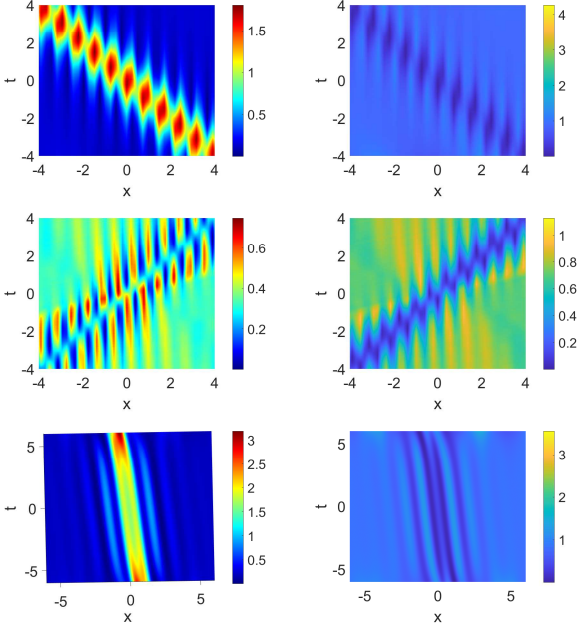


FIG. 7. The results of the numerical simulations of the evolution of BSSs under the action of 2% noise. The initial state is taken as per the analytical solutions (15). The top row corresponds to Fig. 1(a), the middle row corresponds to Fig. 1(b), and the bottom row corresponds to Fig. 2(a).

we have observed the phenomenon of spin oscillations, where the spin-density distribution undergoes periodic oscillations, the stability and frequencies of the oscillations being controlled by the helicoidal SOC. Additionally, we have obtained a composite soliton containing both breathers and BSSs, and analyzed its diverse dynamical behavior. Finally, we studied the nonlinear superposition and interaction between different BSSs, including head-on collisions between solitons with different velocities, and bound states formed by solitons with identical velocities.

In the experiment, a laser beam can be used to generate an optical lattice with the spatially non-uniform helicoidal spin-orbit coupling. By adjusting the intensity and phase of the laser, the spin coupling strength  $\alpha$  and helical rate  $\kappa$  in the system can be controlled. This setup allows the study of nonlinear localized wave excitations in the helicoidal SOC-BEC, including stripe solitons, beating solitons, and BSSs.

In this work, we have not considered the effects of the Zeeman splitting (this effect breaks the integrability of system (1)). As continuation of the work, we will conduct approximate analytical studies for BSSs in system (1) that includes the Zeeman splitting, using methods such as the multiple-scale expansion and variational approximation. Additionally, external potentials (e.g., harmonic-oscillator, parity-time-symmetric, and optical-lattice ones) significantly impact the stability of solitons and the excitation of novel soliton modes. We also plan to further investigate BSSs under the influence of exter-

nal potentials.

## ACKNOWLEDGMENTS

This work was supported by the Natural Science Foundation of Hubei Province of China (Grant No. 2023AFB222) and the National Natural Science Foundation of China (Grant Nos. 11975172, 12261131495 and 12381240286).

## Appendix A: Vector beating stripe solitons (BSSs)

Equation (1) is gauge-equivalent to the Manakov system,

$$i\mathbf{u}_t + \frac{1}{2}\mathbf{u}_{xx} + s(\mathbf{u}^\dagger \mathbf{u})\mathbf{u} = 0, \quad \mathbf{u} = (u_1, u_2)^T, \quad (\text{A1})$$

through the following transformation [47, 61]:

$$\Psi = \mathbf{T}\mathbf{u} = \begin{pmatrix} \nu_+ e^{-i(k_m + \kappa)x} & \nu_- e^{i(k_m - \kappa)x} \\ \nu_- e^{-i(k_m - \kappa)x} & -\nu_+ e^{i(k_m + \kappa)x} \end{pmatrix} \mathbf{u}, \quad (\text{A2})$$

where  $k_m = \sqrt{\alpha^2 + \kappa^2}$  is the effective momentum of the lowest-energy states, and  $\mathbf{T}$  is the spatially non-uniform transformation matrix.

Here, we emphasize that, in the context of two-component BECs, systems comprising two distinct atomic species or different hyperfine states of the same atom can be described by the coupled Gross-Pitaevskii equations (cGPEs) [59], which account for varying intra- and inter-species interaction strengths. When these strengths are equal, and no external potential is present, these cGPEs amount to the Manakov system (A1).

The gauge-equivalent relationship allows one to construct solutions to Eq. (1) on the basis of the exact solutions of the Manakov system.

The Lax pair of the Manakov system is taken as [60]

$$\begin{aligned} \Phi_x &= M\Phi, \quad M \equiv i(\lambda\sigma + U), \\ \Phi_t &= N\Phi, \quad N \equiv i(\lambda^2\sigma + \lambda U) + \frac{1}{2}\sigma(U_x - iU^2), \end{aligned} \quad (\text{A3})$$

where

$$U = \begin{pmatrix} 0 & su_1^* & su_2^* \\ u_1 & 0 & 0 \\ u_2 & 0 & 0 \end{pmatrix}, \quad \sigma = \text{diag}(1, -1, -1). \quad (\text{A4})$$

To derive the BSSs, we begin with the plane waves, taken as the zero-order seed solutions:

$$u_1^{(0)} = ae^{i\theta_1}, \quad u_2^{(0)} = 0, \quad (\text{A5})$$

where

$$\theta_j = k_j x + (sa^2 - \frac{1}{2}k_j^2)t. \quad (\text{A6})$$

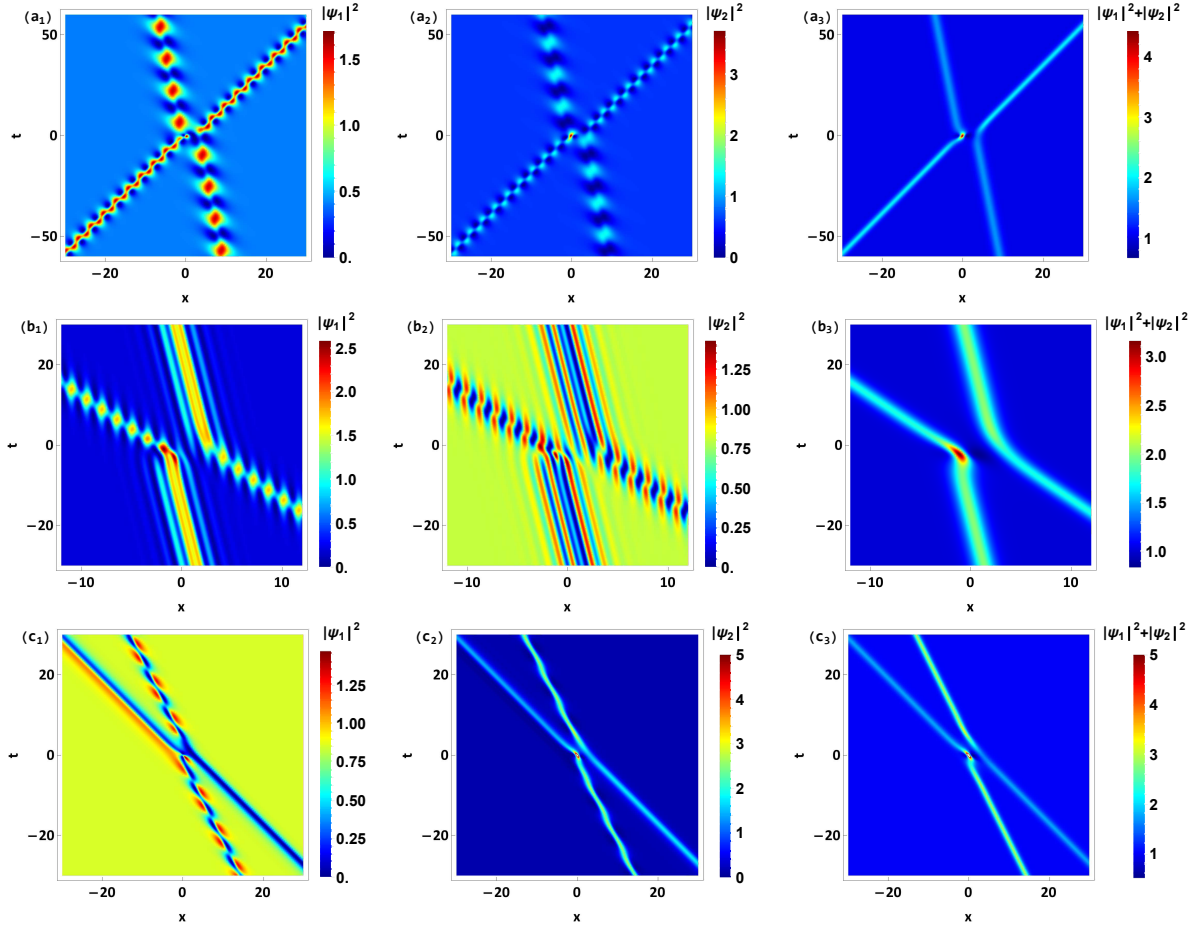


FIG. 8. (a) The interaction between two beating stripe solitons with  $k_1 = \frac{1}{2}$ ,  $\lambda_1 = -\frac{1}{4} + \frac{4}{5}i$ ,  $\lambda_2 = -\frac{1}{4} + i$ ,  $\alpha = 0.5$ , and  $\kappa = 0.1$ ; (b) The interaction between a beating stripe soliton and a vibrating dark-bright soliton pair with  $k_1 = -0.1$ ,  $\lambda_1 = 0.05 - i$ ,  $\lambda_2 = 0.05 + \frac{\sqrt{3}}{2}i$ ,  $\alpha = 2$ , and  $\kappa = 1.5$ ; (c) The interaction between a beating stripe soliton and non-vibrating dark-bright soliton pair with  $k_1 = -0.5$ ,  $\lambda_1 = 0.25 + \frac{\sqrt{3}}{2}i$ ,  $\lambda_2 = 0.25 + 1.05i$ ,  $\alpha = -\kappa = \frac{\sqrt{2}}{8}$ . The other parameters are  $s = 1$ ,  $a = 1$ ,  $l_{j1} = l_{j3} = 1$ , and  $l_{j2} = 0$  ( $j = 1, 2$ ).

The substitution of the above-mentioned seed solutions (A5) in the Lax pair (A3) gives rise to the fundamental eigenfunction solution,

$$\Phi_1 = (\phi, \varphi, \psi)^T = GHKLe^{-i[\lambda_1 x + (sa^2 + \lambda_1^2)t]}, \quad (\text{A7})$$

where  $G = \text{diag}(1, ae^{i\theta_1}, e^{i\theta_2})$ ,  $L = (l_1, l_2, l_3)^T$ ,  $K = \text{diag}(e^{-iA(\mu_1)}, e^{-iA(\mu_2)}, e^{-iA(k_2)})$ , and

$$H = \begin{pmatrix} 1 & 1 & 0 \\ \frac{1}{k_1 - \mu_1} & \frac{1}{k_1 - \mu_2} & 0 \\ 0 & 0 & 1 \end{pmatrix}, \quad (\text{A8})$$

with  $l_j$  ( $j = 1, 2, 3$ ) representing the characteristic parameters of the initial soliton and  $A(\mu) = \mu(x - \frac{\mu}{2}t)$ .

Then, the fundamental BSS solutions of Eq. (1) can be derived by utilizing the gauge transformation (A2) and the following Darboux transformation of Manakov system

$$U[1] = U + \frac{\lambda_1^* - \lambda_1}{\mathbf{y}_1^\dagger \Lambda \mathbf{y}_1} [\mathbf{y}_1 \mathbf{y}_1^\dagger \Lambda, \sigma], \quad (\text{A9})$$

where  $\mathbf{y}_1 \equiv v_1(x, t)\Phi_1$  with  $v_1(x, t)$  being a nonzero complex function,  $\Lambda = \text{diag}(1, s, s)$  and commutator of quantum operators is fixed as  $[A, B] = AB - BA$ . Substituting the eigenfunction (A7) into the Darboux transform (A9) with  $v_1(x, t) = e^{i[\lambda_1 x + (sa^2 + \lambda_1^2)t]}$  and combining the gauge transformation (A2), we can obtain the BSS solutions of Eq. (1) as explicitly shown by Eq. (5).

## Appendix B: $N$ -th-order beating stripe solitons (BSSs)

Utilizing the plane-wave zero-order seed solutions (A5) as the starting point, we can derive the  $N$ -th-order BSS solutions of Eq. (1) by means of the gauge transform (A2) and application of the following  $N$ -th-order Darboux transform, which is specific to the Manakov system:

$$U[N] = U + [\sigma, Y \Sigma^{-1} Y^\dagger \Lambda], \quad (\text{B1})$$

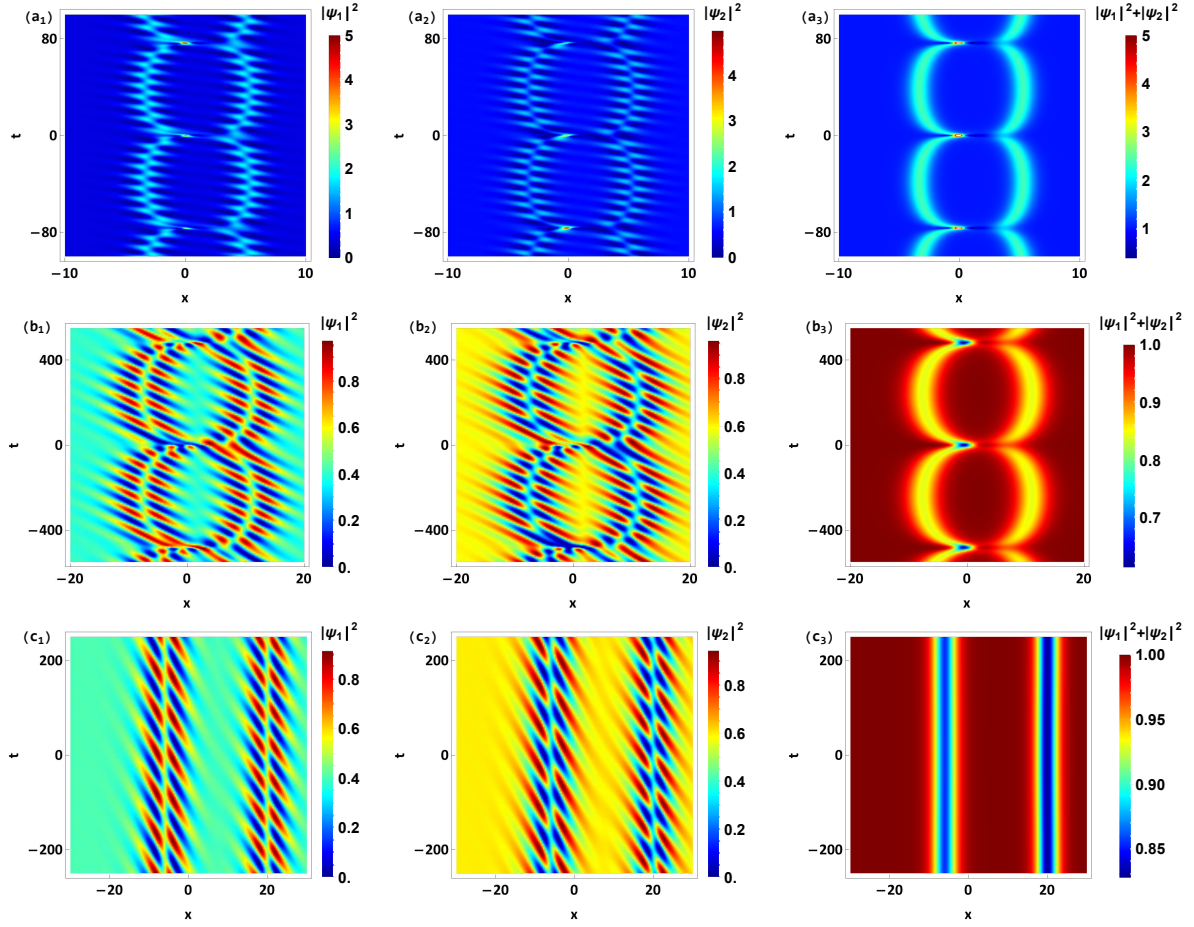


FIG. 9. Bound and parallel states of two beating stripe solitons with parameters (a)  $s = 1$ ,  $\lambda_1 = 1.01i$ ,  $\lambda_2 = 1.02i$ ; (b)  $s = -1$ ,  $\lambda_1 = -i$ ,  $\lambda_2 = -1.12i$ ; (c) the same parameters as in (b), except for  $l_{11} = 100$ . The other parameters are  $a = 1$ ,  $k_1 = 0$ ,  $\alpha = 0.5$ ,  $\kappa = 0.1$ ,  $l_{j1} = l_{j3} = 1$ , and  $l_{j2} = 0$  ( $j = 1, 2$ ).

where  $\mathbf{Y} = (\mathbf{y}_1, \mathbf{y}_2, \dots, \mathbf{y}_N)$  with  $\mathbf{y}_j \equiv v_j(x, t)\Phi_j$ ,  $\Phi_j$  is the eigenfunction solution of Lax pair (A3) at  $\lambda = \lambda_j$  with the plane-wave zero-seed solutions (A5), and  $\Sigma = (\Sigma_{ij})_{N \times N}$  with  $\Sigma_{ij} = \mathbf{y}_i^\dagger \Lambda \mathbf{y}_j / (\lambda_j - \lambda_i^*)$ . The eigenfunction solution  $\Phi_j$  has the form

$$\Phi_j = GH_j K_j L_j e^{-i[\lambda_j x + (sa^2 + \lambda_j^2)t]}, \quad (\text{B2})$$

where  $G = \text{diag}(1, ae^{i\theta_1}, e^{i\theta_2})$ ,  $L_j = (l_{j1}, l_{j2}, l_{j3})^T$ ,  $K_j = \text{diag}(e^{-iA(\mu_{j1})}, e^{-iA(\mu_{j2})}, e^{-iA(k_2)})$ , and

$$H_j = \begin{pmatrix} 1 & 1 & 0 \\ \frac{1}{k_1 - \mu_{j1}} & \frac{1}{k_1 - \mu_{j2}} & 0 \\ 0 & 0 & 1 \end{pmatrix}, \quad (\text{B3})$$

with  $l_{jk}$  ( $k = 1, 2, 3$ ) being complex parameters, and  $A(\mu) = \mu(x - \frac{\mu}{2}t)$ . The eigenvalues  $\mu_{j1}$  and  $\mu_{j2}$  are solutions of the following quadratic equation with spectral parameter  $\lambda_j$

$$\mu^2 + (2\lambda_j - k_1)\mu - sa^2 - 2k_1\lambda_j = 0. \quad (\text{B4})$$

Substituting the  $N$ -th-order solutions (B1) into gauge transform (A2), we can obtain the  $N$ -th-order BSSs for the original Eq. (1).

- [1] C. Qu, L. P. Pitaevskii, and S. Stringari, Magnetic Solitons in a Binary Bose-Einstein Condensate, Phys. Rev. Lett. **116**, 160402 (2016).  
 [2] A. Farolfi, D. Trypogeorgos, C. Mordini, G. Lamporesi, and G. Ferrari, Observation of Magnetic Solitons in Two-

- Component Bose-Einstein Condensates, Phys. Rev. Lett. **125**, 030401 (2020).  
 [3] X. Chai, D. Lao, K. Fujimoto, R. Hamazaki, M. Ueda, and C. Raman, Magnetic Solitons in a Spin-1 Bose-Einstein Condensate, Phys. Rev. Lett. **125**, 030402

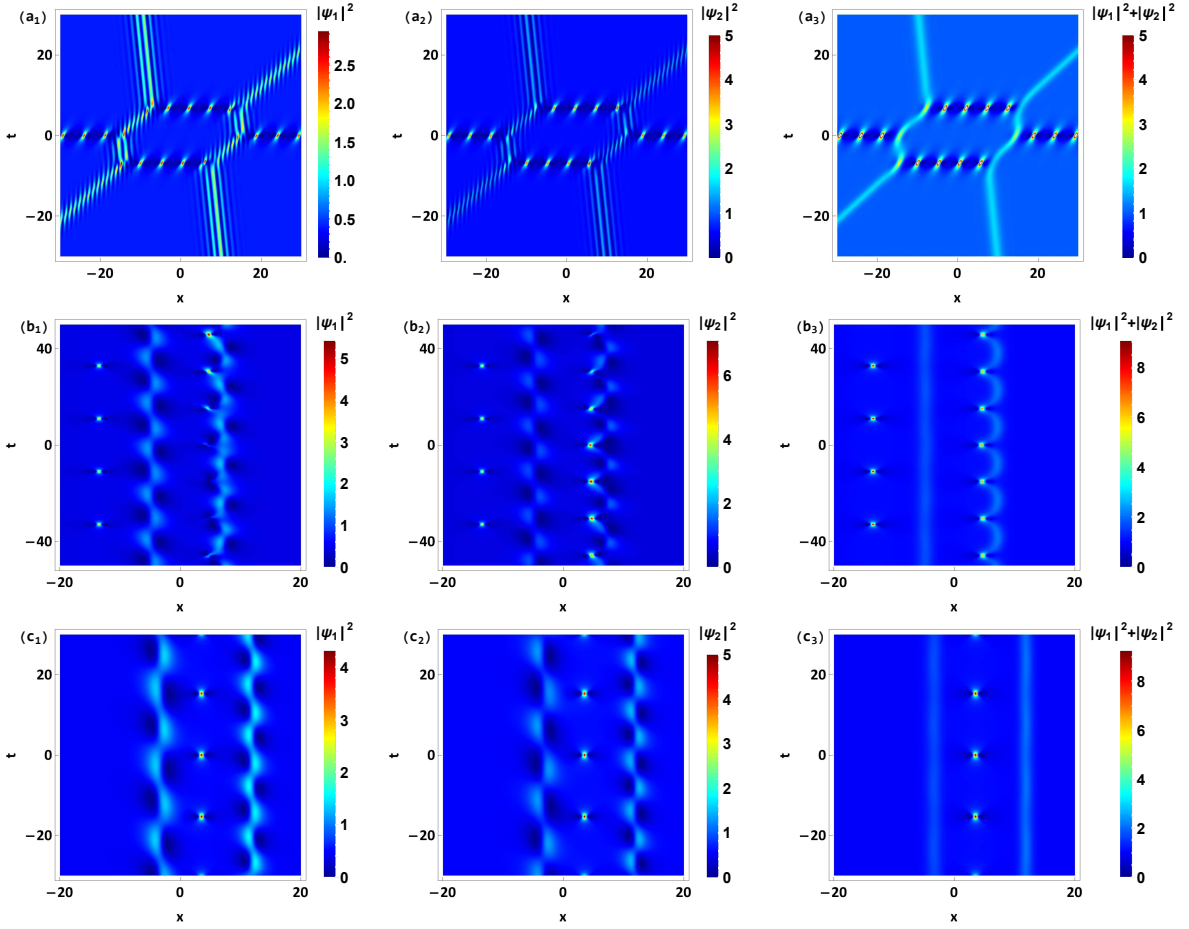


FIG. 10. (a) Interactions between two Y-shaped composite beating stripe solitons with  $k_1 = 0.5$ ,  $\lambda_1 = -0.25 + 0.8i$ ,  $\lambda_2 = -0.25 - 0.801i$ ,  $\alpha = \sqrt{6}$ ,  $\kappa = 0.5$ ,  $l_{13} = -l_{23} = 0.01$ . (b) Two parallel composite beating stripe solitons with  $k_1 = 0$ ,  $\lambda_1 = 1.01i$ ,  $\lambda_2 = -1.02i$ ,  $\alpha = 0.1$ ,  $\kappa = 0.01$ ,  $l_{12} = 40$ . (c) Mutually parallel a composite beating stripe soliton and a single beating stripe one with  $k_1 = 0$ ,  $\lambda_1 = -1.02i$ ,  $\lambda_2 = i$ ,  $\alpha = 0.1$ ,  $\kappa = 0.01$ ,  $l_{12} = 0.3$ ,  $l_{22} = 10000$ . The other parameters are  $s = 1$ ,  $a = 1$ , and  $l_{11} = l_{21} = 1$ .

- (2020).
- [4] E. Kengne, W.-M. Liu, and B. A. Malomed, Spatiotemporal engineering of matter-wave solitons in Bose-Einstein condensates, *Phys. Rep.* **899**, 1 (2021).
- [5] L.-Z. Meng, Y.-H. Qin and L.-C. Zhao, Spin solitons in spin-1 Bose-Einstein condensates, *Commun. Nonlinear Sci. Numer. Simulat.* **109**, 106286 (2022).
- [6] N. Mao and L.-C. Zhao, Exact analytical soliton solutions of N-component coupled nonlinear Schrödinger equations with arbitrary nonlinear parameters, *Phys. Rev. E* **106**, 064206 (2022).
- [7] P. G. Kevrekidis, D. J. Frantzeskakis, and R. Carretero-González, *Emergent Nonlinear Phenomena in Bose-Einstein Condensates: Theory and Experiment* (Springer-Verlag, Heidelberg, 2008).
- [8] S. V. Manakov, On the theory of two-dimensional stationary self-focusing of electromagnetic waves, *Sov. Phys. JETP*, **38**, 248 (1974).
- [9] X.F. Zhang, X.H. Hu, X.-X. Liu, and W. M. Liu, Vector solitons in two-component Bose-Einstein condensates with tunable interactions and harmonic potential, *Phys. Rev. A* **79**, 033630 (2009).
- [10] H. E. Nistazakis, D. J. Frantzeskakis, P. G. Kevrekidis, B. A. Malomed, and R. Carretero-González, Bright-dark soliton complexes in spinor Bose-Einstein condensates, *Phys. Rev. A* **77**, 033612 (2008).
- [11] Majed O. D. Alotaibi and L. D. Carr, Dynamics of dark-bright vector solitons in Bose-Einstein condensates, *Phys. Rev. A* **96**, 013601 (2017).
- [12] L. Ling, L. C. Zhao, B. Guo, Darboux transformation and multi-dark soliton for N-component NLS, *Nonlinearity* **28**, 3243-3261 (2015).
- [13] Th. Busch, and J. R. Anglin, Dark-bright solitons in inhomogeneous Bose-Einstein condensates, *Phys. Rev. Lett.* **87**, 010401 (2001).
- [14] C. Yin, N. G. Berloff, V. M. Perez-Garcia, V. A. Brazhnyi, and H. Michinel, Coherent atomic soliton molecules for matter-wave switching, *Phys. Rev. A* **83**, 051605 (2011).
- [15] M. Vijayajayanthi, T. Kanna, and M. Lakshmanan, Bright-dark solitons and their collisions in mixed-coupled nonlinear Schrödinger equations, *Phys. Rev. A* **77**, 013820 (2008).

- [16] V. Achilleos, P. G. Kevrekidis, V. M. Rothos, and D. J. Frantzeskakis, Statics and dynamics of atomic dark-bright solitons in the presence of impurities, *Phys. Rev. A* **84**, 053626 (2011).
- [17] V. Achilleos, D. Yan, P. G. Kevrekidis, and D. J. Frantzeskakis, Dark-bright solitons in Bose-Einstein condensates at finite temperatures, *New J. Phys.* **14**, 055006 (2012).
- [18] E. T. Karamatskos, J. Stockhofe, P. G. Kevrekidis and P. Schmelcher, Stability and tunneling dynamics of a dark-bright soliton pair in a harmonic trap, *Phys. Rev. A* **91**, 043637 (2015).
- [19] G. C. Katsimiga, P. G. Kevrekidis, B. Prinari, G. Biondini and P. Schmelcher, Dark-bright soliton pairs: Bifurcations and collisions, *Phys. Rev. A* **97**, 043623 (2018).
- [20] C. Becker, S. Stellmer, P. Soltan-Panahi, S. Dörscher, M. Baumert, E.-M. Richter, J. Kronjäger, K. Bongs, and K. Sengstock, Oscillations and interactions of dark and dark-bright solitons in Bose-Einstein condensates, *Nature Phys.* **4**, 496 (2008).
- [21] Z. Chen, M. Segev, T. H. Coskun, D. N. Christodoulides, Yu. S. Kivshar, and V. V. Afanasjev, Incoherently coupled dark-bright photorefractive solitons, *Opt. Lett.* **21**, 1821 (1996).
- [22] C. Hamner, J. J. Chang, P. Engels, and M. A. Hoefer, Generation of dark-bright soliton trains in superfluid-superfluid counterflow, *Phys. Rev. Lett.* **106**, 065302 (2011).
- [23] D. Yan, J. J. Chang, C. Hamner, P. G. Kevrekidis, P. Engels, V. Achilleos, D. J. Frantzeskakis, R. Carretero-González, and P. Schmelcher, Multiple dark-bright solitons in atomic Bose-Einstein condensates, *Phys. Rev. A* **84**, 053630 (2011).
- [24] N. N. Akhmediev, W. Krolikowski, and A. W. Snyder, Partially Coherent Solitons of Variable Shape, *Phys. Rev. Lett.* **81**, 4632 (1998).
- [25] N. Akhmediev and A. Ankiewicz, Partially Coherent Solitons on a Finite Background, *Phys. Rev. Lett.* **82**, 2661 (1999).
- [26] N. Akhmediev, A. Ankiewicz, Multi-soliton complexes, *Chaos* **10**, 600 (2000).
- [27] S. Stalin, R. Ramakrishnan, M. Senthilvelan, and M. Lakshmanan, Nondegenerate Solitons in Manakov System, *Phys. Rev. Lett.* **122**, 043901 (2019).
- [28] R. Ramakrishnan, S. Stalin, and M. Lakshmanan, Nondegenerate solitons and their collisions in Manakov systems, *Phys. Rev. E* **102**, 042212 (2020).
- [29] Y.-H. Qin, L.-C. Zhao, Z.-Q. Yang, and L. Ling, Multivalley dark solitons in multicomponent Bose-Einstein condensates with repulsive interactions, *Phys. Rev. E* **104**, 014201 (2021).
- [30] Q. H. Park, H. J. Shin, Systematic construction of multicomponent optical solitons, *Phys. Rev. E* **61**, 3093 (2000).
- [31] D. Yan, J. J. Chang, C. Hamner, M. A. Hoefer, P. G. Kevrekidis, P. Engels, V. Achilleos, D. J. Frantzeskakis, and J. Cuevas, Beating dark-dark solitons in Bose-Einstein condensates, *J. Phys. B* **45**, 115301 (2012).
- [32] V. Achilleos, D. J. Frantzeskakis, and P. G. Kevrekidis, Beating dark-dark solitons and Zitterbewegung in spin-orbit-coupled Bose-Einstein condensates, *Phys. Rev. A* **89**, 033636 (2014). 2014, 89(3): 033636.
- [33] E. G. Charalampidis, P. G. Kevrekidis, D. J. Frantzeskakis, B. A. Malomed, Dark-bright solitons in coupled nonlinear Schrödinger equations with unequal dispersion coefficients, *Phys. Rev. E* **91**, 012924 (2015).
- [34] L. C. Zhao, Beating effects of vector solitons in Bose-Einstein condensates, *Phys. Rev. E* **97**, 062201 (2018).
- [35] X. L. Li, L. Z. Meng, L. C. Zhao, Asymmetric solitons induced by transition and beating effects, *J. Phys. B: At. Mol. Opt. Phys.* **56**, 245301 (2023)
- [36] C. Liu, W. J. Che, N. Akhmediev, Classification of beating solitons, their physical spectra, and second-order nonlinear superpositions, *Phys. Rev. E* **110**, 044210 (2024).
- [37] M. A. Hoefer, J. J. Chang, C. Hamner, and P. Engels, Dark-dark solitons and modulational instability in miscible two-component Bose-Einstein condensates, *Phys. Rev. A* **84**, 041605 (R) (2011).
- [38] E. G. Charalampidis, W. Wang, P. G. Kevrekidis, D. J. Frantzeskakis, and J. Cuevas-Maraver, SO(2)-induced breathing patterns in multicomponent Bose-Einstein condensates, *Phys. Rev. A* **93**, 063623 (2016).
- [39] W. Wang, L.-C. Zhao, E. G. Charalampidis, and P. G. Kevrekidis, Dark-dark soliton breathing patterns in multicomponent Bose-Einstein condensates, *J. Phys. B: At. Mol. Opt. Phys.* **54**, 055301 (2021).
- [40] A. Gelash and A. Raskovalov, Vector breathers in the Manakov system, *Stud. Appl. Math.* **150**, 841 (2023).
- [41] O. Morsch, and M. Oberthaler, Dynamics of Bose-Einstein condensates in optical lattices, *Rev. Mod. Phys.* **78**, 179 (2006)
- [42] Y. V. Kartashov, B. A. Malomed, and L. Torner, Solitons in nonlinear lattices, *Rev. Mod. Phys.* **83**, 247 (2011)
- [43] C. M. de Sterke, and J. E. Sipe, Envelope-function approach for the electrodynamics of nonlinear periodic structures, *Phys. Rev. A* **38**, 5149 (1988).
- [44] V. V. Konotop and M. Salerno, Modulational instability in Bose-Einstein condensates in optical lattices, *Phys. Rev. A* **65**, 021602 (2002).
- [45] H. Sakaguchi, and B. A. Malomed, Matter-wave solitons in nonlinear optical lattices, *Phys. Rev. E* **72**, 046610 (2005).
- [46] Y. V. Kartashov, V. A. Vysloukh, and L. Torner, Soliton shape and mobility control in optical lattices, *Prog. Opt.* **52**, 63 (2009).
- [47] Y. V. Kartashov, and V. V. Konotop, Solitons in Bose-Einstein condensates with helicoidal spin-orbit coupling, *Phys. Rev. Lett.* **118**, 190401 (2017)
- [48] Y. V. Kartashov, V. V. Konotop, M. Modugno, and E. Ya. Sherman, Solitons in inhomogeneous gauge potentials: integrable and nonintegrable dynamics, *Phys. Rev. Lett.* **122**, 064101 (2019).
- [49] P. Fang, and J. Lin, Soliton in Bose-Einstein condensates with helicoidal spin-orbit coupling under a Zeeman lattice, *Phys. Rev. E* **109**, 064219 (2024).
- [50] M. J. Ablowitz and J. F. Ladik, Nonlinear differential-difference equations and Fourier analysis, *J. Math. Phys.* **17**, 1011-1018 (1976).
- [51] O. F. Oxtoby and I. V. Barashenkov, Moving solitons in the discrete nonlinear Schrödinger equation, *Phys. Rev.* **76**, 036603 (2017).
- [52] Y. Zhang, G. Chen, and C. Zhang, Tunable spin-orbit coupling and quantum phase transition in a trapped Bose-Einstein condensate, *Sci. Rep.* **3**, 1937 (2013).
- [53] K. Jiménez-García, L. J. LeBlanc, R. A. Williams, M. C. Beeler, C. Qu, M. Gong, C. Zhang, and I. B. Spielman, Tunable spin-orbit coupling via strong driving in ultracold-atom systems, *Phys. Rev. Lett.* **114**, 125301 (2015).

- (2015).
- [54] X. Luo, L. Wu, J. Chen, Q. Guan, K. Gao, Z.-F. Xu, L. You, and R. Wang, Tunable atomic spin-orbit coupling synthesized with a modulating gradient magnetic field, *Sci. Rep.* **6**, 18983 (2016).
- [55] M. C. Rechtsman, J. M. Zeuner, Y. Plotnik, Y. Lumer, D. Podolsky, F. Dreisow, S. Nolte, M. Segev, and A. Szameit, Photonic Floquet topological insulators, *Nature (London)* **496**, 196 (2013).
- [56] S. V. Samsonov, A. D. R. Phelps, V. L. Bratman, G. Burt, G. G. Denisov, A. W. Cross, K. Ronald, W. He, and H. Yin, Compression of frequency-modulated pulses using helically corrugated waveguides and its potential for generating multigigawatt rf radiation, *Phys. Rev. Lett.* **92**, 118301 (2004).
- [57] G. Burt, S. V. Samsonov, K. Ronald, G. G. Denisov, A. R. Young, V. L. Bratman, A. D. R. Phelps, A. W. Cross, I. V. Konoplev, W. He, J. Thomson, and C. G. Whyte, Dispersion of helically corrugated waveguides: Analytical, numerical, and experimental study, *Phys. Rev. E* **70**, 046402 (2004).
- [58] J. Dalibard, F. Gerbier, G. Juzeliunas, and P. Öhberg, Colloquium: Artificial gauge potentials for neutral atoms, *Rev. Mod. Phys.* **83**, 1523 (2011).
- [59] P. G. Kevrekidis, D. J. Frantzeskakis, and R. Carretero-González, *The defocusing nonlinear Schrödinger equation: from dark solitons to vortices and vortex rings* (Society for Industrial and Applied Mathematics, 2015).
- [60] B. Guo, L. Ling, and Q. P. Liu, Nonlinear Schrödinger equation: generalized Darboux transformation and rogue wave solutions, *Phys. Rev. E* **85**, 026607 (2012).
- [61] C. C. Ding, Q. Zhou, and B. A. Malomed, Ultra-high-amplitude Peregrine solitons induced by helicoidal spin-orbit coupling, *Phys. Rev. Research* **6**, L032036 (2024).